Applied Surface Science 607 (2023) 154925

Contents lists available at ScienceDirect

Applied Surface Science

journal homepage: www.elsevier.com/locate/apsusc

Full Length Article

Self-assembled microstructures with localized graphene domains in an epoxy blend and their related properties

Suihua He [a], Hartmut Stadler [b], Xuankai Huang [c], Xiang Zheng [d], Guanjie Yuan [d], Martin Kuball [d], Miriam Unger [b], Carwyn Ward [a], Ian Hamerton [a,*]

[a] Bristol Composites Institute, Department of Aerospace Engineering, School of Civil, Aerospace, and Mechanical, Engineering, Queen's Building, University of Bristol, University Walk, Bristol BS8 1TR, UK
[b] Bruker Nano Surfaces & Metrology, Östliche Rheinbrückenstrasse 49, 76187 Karlsruhe, Germany
[c] Department of Chemistry, School of Physical and Chemical Sciences, Queen Mary University of London, Mile End Road, London E1 4NS, UK
[d] Centre for Device Thermography and Reliability, H.H. Wills Physics Laboratory, University of Bristol, Bristol BS8 1TL, UK

ARTICLE INFO

Keywords:
Self-assembly
Microstructures
Graphene domains
Epoxy resin
Nanocomposites

ABSTRACT

Locating nanoparticles in selected areas *via* the mixing of two immiscible polymers is widely studied for achieving nanocomposites with next-level performance, however, the formation of a phase-separated domain constructed with nanofillers from entirely miscible molecules is rarely achieved in the literature. Here we demonstrate a method to fabricate a self-constructed bi-continuous phase structure with localized amine-functionalized graphene nanoplatelets (A-GNPs) in a liquid processable multi-component epoxy blend. Atomic force microscopy infrared spectroscopy (AFM-IR) was employed to identify the compositions of the phase-separated microdomains formed during self-assembly by A-GNP in the multi-component epoxy blend, with incorporating 1-(2-aminoethyl) piperazine (AEPIP) found to be the driving force for the formation of the graphene microdomains. Nanoindentation measurements show that a Young's modulus of 6.3 GPa for the graphene domain was achieved, which is nearly twice that of the epoxy resin (3.2 GPa). Transient thermoreflectance results indicate that the thermal conductivity of nanocomposite with phase-separated graphene domain reached 0.48 W/mK, exhibiting a significant enhancement (70%) when compared to epoxy resin, while maintaining excellent dielectric properties. Overall, this study provides a simple and effective route to fabricate phase-separated microstructure with nanoparticles from a liquid processable nanocomposite blend, which shows the great potential of this promising new approach to fabricate nanocomposite films with excellent performance for microelectronics applications.

1. Introduction

The rapid development of electronic devices used in cutting-edge fields such as the aerospace industry and 5G technology, has led to demands for advanced packaging materials with better performance, longer lifetimes, and higher reliability. To solve the issues raised by the increase of power density in smaller, more densely packed microelectronic devices, dielectric polymer composites with high thermal conductivity and low crosstalk are considered to be promising candidates [1-3]. Thermoset epoxy resins with crosslinked molecular architectures have been regarded as one of the ideal polymer matrices for the fabrication of microelectronic packaging materials, due to their reliable mechanical properties, high dielectric strength and low dielectric loss properties, thermal stability and easy processing [2,4]. However, further improvements in the design and development of dielectric polymer nanocomposites with tailored properties are needed to fulfil the requirements of the aforementioned applications and the addition of nanofillers to polymer matrices has been widely reported as one of the most effective approaches for the preparation of nanocomposites with multi-functional properties [5-8].

Compared with carbon nanotubes (CNTs), graphene, which has a higher surface-to-volume ratio and a lower production cost [9], exhibits excellent thermal and mechanical properties; emerging to be the desired filler for high-performance epoxy-based nanocomposites [10,11]. However, the full potential of these composites has yet to be fully realized, due in part to the difficulties of dispersing carbonaceous fillers

* Corresponding author.
E-mail address: ian.hamerton@bristol.ac.uk (I. Hamerton).

https://doi.org/10.1016/j.apsusc.2022.154925
Received 20 June 2022; Received in revised form 1 September 2022; Accepted 12 September 2022
Available online 18 September 2022

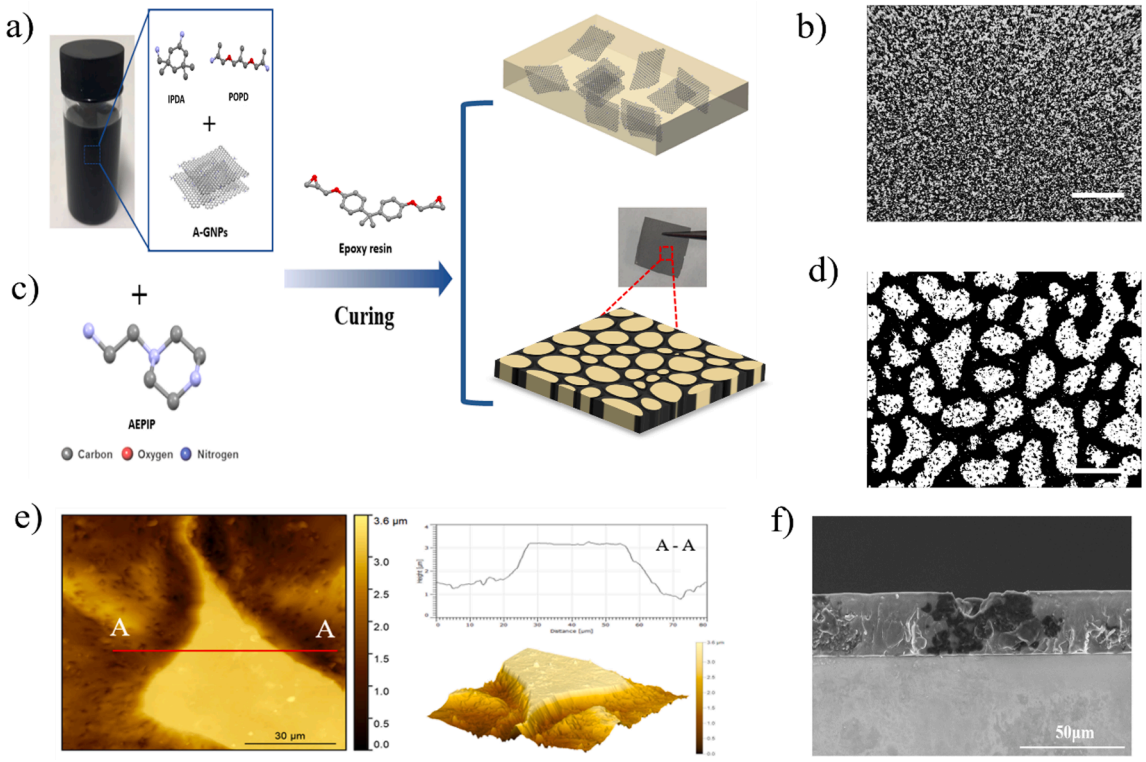

Fig. 1. Fabrication process and structure of phase-separated domain with A-GNP, **a)** A-GNPs dispersed in RS-MH137 via ultra-sonication and **c)** AEPIP incorporated in the mixture before mixing with Epoxy blend for fabricating nanocomposite films. **b, d)** Corresponding optical images of the films fabricated by the multi-component blend of Epoxy/MH137/A-GNPs and Epoxy/MH137-AEPIP/A-GNPs, respectively (Scale bar: 100 μm). **e)** AFM images and virtual details of final optically reconstructed morphology. **f)** Corresponding SEM image of the cross-section.

in polymer matrices[12,13]. In order to form a highly efficient filler conductive network, the structural design of the composites with the selective distribution of nanoparticles is considered to be one of the most promising techniques offering the potential to fabricate spontaneously organized nano-micro scale structures [5,14,15]. The distinct properties of the nanoparticles can be integrated into assemblies of the nano-micro domain, which leads to novel superstructures with unique combinations of properties.

Selective localization of nanoparticles in shaping the final properties of thermoplastic (TP)/ thermoset (TS) systems has been widely studied in the past decade. There are now a number of reports illustrating the preparation of multifunctional epoxy/thermoplastic composites by incorporating self-assembling nanofiller networks within a specific continuous domain [15-17]. Zhang *et al.* [15] prepared epoxy/polyethersulphone (PES) nanocomposites through the incorporation of graphene nanoplatelets (GNPs) to yield a self-assembled filler network *via* reaction-induced phase separation (RIPS); the resulting composites exhibited almost a 3.5-fold enhancement in thermal conductivity when compared to the pure epoxy, or 52% compared to the epoxy/GNP composite containing no PES.

Similarly, Jin *et al.* [16] used boron nitride nanosheets (BNNSs) to develop an effective and facile method to force the construction of a three-dimension thermal conductive pathway in BNNSs-NH_2/epoxy/polyetherimideternary blends *via* RIPS. The resulting nanocomposites displayed an impressive 83% enhancement in through-plane thermal conductivity (from 0.18 to 0.33 W m^{-1} K^{-1}) with a modest (1 wt%) BNNSs-NH_2 loading. However, the lower thermal stability and high viscosity of the resulting blends caused by the high molecular weight of the TP used in the blend limit their potential applications to those where infusion processing is not commonly used. Additionally, while modern epoxy blends containing TP films and particles may display high fracture toughness, this usually comes at the expense of matrix stiffness. For example, a composite prepared from a third-generation toughened epoxy prepreg HexPly M21/HexTow IM7 displays a compression after impact value of 30 J = 298 MPa, and interlaminar shear strength of 110 MPa, with a cured dry T_g of 195 °C, but the compression properties remain relatively modest (modulus 148 GPa, strength 1790 MPa) [18].

Selective localization of nanofillers in TS blends is rarely achieved and consequently, very few literature examples show the successful development of phase-separated structures *via* RIPS in TS/TS blends, although the use of benzoxazine (BOX)/cyanate ester (CE) [19], BOX/bismaleimide (BMI) [20-23] and BOX/epoxy resin blends have been reported. Wang *et al.* [20] fabricated BOX/BMI blends with bi-continuous phase structures *via* the use of an imidazole initiator and found that both the phase separation and phase morphology were determined mainly by the viscosity parameters of blends. Zhao *et al.* [24,25] investigated the RIPS behaviour in BOX/epoxy resin systems and found that realizing sequential polymerization of the epoxy resin and BOX either by increasing the initial molecular weight of epoxy resin or by adding imidazole achieved a phase-separated structure. However, this additional level of complexity means that TS/TS blends are rarely studied in detail and a systematic study of the mechanism of phase separation behaviour in TS/TS systems with selective localization of nanofillers remains largely unexplored.

Recently, Huang *et al.* [26] reported that the selective location of multiwall CNTs (MWCNTs) in the continuous domain of an epoxy nanocomposite blend dramatically improved the measured electrical properties of epoxy composites (with an ultra-low percolation threshold of ~ 0.032 wt% MWCNT) while maintaining excellent tensile strength (37 ± 1.28 MPa) and modulus (2.88 ± 0.14 GPa). Although the researchers offered much insight into the structure, properties, and phase behaviour of TS/TS blends, the study relied heavily on imaging (transmission electron microscopy, TEM, scanning electron microscopy, SEM, and optical microscopy) [27,28] and thermal analysis techniques such as dynamic mechanical thermal analysis [29]. Whilst offering powerful evidence to characterize the resins and identify the phase behaviour and

selective localization of MWCNT in the TS/TS system, the study lacked direct evidence about the chemical distribution of each component at the molecular level and this forms the impetus for the current study.

Atomic force microscopy-infrared (AFM-IR) spectroscopy is a hyphenated analytical technique, that has emerged recently, and combines the high spatial resolution of AFM with the chemical analysis capability of conventional IR spectroscopy [30,31]. Specifically, in polymer science, it is believed that the application of AFM-IR could play an important role in understanding the mechanism of the heterogeneity structure in the polymer blends [32-35]. In the present work, we propose a facile and widely applicable methodology for preparing a nanocomposite film with self-assembled nanofiller domains, exhibiting high thermal conductivity and mechanical properties while maintaining excellent dielectric properties. Specifically, we report the use of AFM-IR spectroscopy to identify the chemical distribution of a self-assembled phase domain with selective localization of amine-functionalised GNPs (A-GNPs) during the cure of a liquid processable commercial epoxy blend for investigating the plausible mechanisms, which might enable the controlling of the phase structure with selective localization of nanofillers in TS systems.

2. Experimental section

2.1. Materials

Component A**,** RS-M135 (PRF Composites, UK) is an epoxy resin produced from bisphenol A diglycidyl ether (DGEBA) (CAS No. 25068-38-6) with a number average molecular weight, $M_n < 700$ g/mol. (70–90 % w/w) and containing an added proportion of 1,6-hexanediol diglycidyl ether (DEGH) (CAS No. 16096-31-4) as a reactive diluent. Component B, RS-MH137 (PRF Composites, UK), is a curing agent that contains (a) 3-aminomethyl-3,5,5-trimethylcyclohexylamine (or isophorodiamine, IPDA) (CAS No. 2855-13-2) 35–50 % w/w, and (b) polyoxypropylenediamine (CAS No. 9046-10-0) (denoted POPD) 50–70 % w/w. Component C, 1-(2-aminoethyl) piperazine (AEPIP) (CAS No. 140-31-8) was purchased from Sigma Aldrich. The chemical structure of the main components used appears in Fig. 1. Amine-functionalized graphene nanoplatelets (A-GNPs) with a mean diameter of 2 μm and thickness under 4 nm were purchased from Cheap Tubes Inc., USA and used as reinforcement in this study (Fig.S1a). According to the manufacturer, these GNPs were produced by mechanical exfoliation process and then surface modified with > 7% primary amino (NH_2) functional groups (the corresponding IR spectrum shown in Fig.S1b). All the materials in this study were used as received without further purification.

2.2. Sample preparation

To process the materials in the present study, the A-GNPs (3 wt%) were dispersed in a blend containing the three curing agents in a specified appropriate ratio by sonication probe in a water bath at room temperature for 1 h. Before the mixing process was commenced, the neat epoxy was degassed *via* a vacuum line at 25 °C for 10 mins. The ratio of epoxy resin to total curing agent was maintained at a 10:3 wt ratio for all samples.

As shown in Fig. 1, two types of reinforced sample were made, first blendwas composed of a mixture of components A and B to fabricate a composite blend; second blend was cured by incorporating a mixture of curing agents with components B and C in a 7:3 wt ratio. The blends were then mixed by using a mechanical stirrer for 10 mins at 1000 rpm. Finally, the epoxy/A-GNPs composite films were fabricated by repeated spin-coating followed by a post-cure process. Briefly, the epoxy/A-GNPs mixture was spin-coated on a glass substrate with a rotation speed of 1500 rpm for 1 min. The (nano)composites films were kept at room temperature for 60 mins before a post-cure process (60 °C for 4hrs) was employed.

2.3. Characterization

2.3.1. Imaging characterization of phase structure

The distribution and dispersion of the GNPs in the epoxy matrix on a larger scale were studied using an optical transmission microscope (Zeiss Axio Imager 2, Carl Zeiss MicroImaging GmbH, Jena, Germany). Representative images were captured on the microscope and then processed using ImageJ.(https://imagej.net/downloads). Atomic Force Microscopy (AFM) images were collected using a Dimension XR (Bruker, Santa Barbara) with an Icon scanner, operating in peak force tapping mode (nominal spring constant 0.4 N/m, peak resonant frequency of 2 kHz). AFM images were thresholded in order to obtain binary images and evaluate the characteristics of different domains and only height images were recorded. AFM images were processed by Gwyddion (version 2.59, http://gwyddion.net/), and the 3D topology images, and a virtual detail of cross-section were generated accordingly. Scanning electron microscopy (SEM) micrographs (TM3030Plus, Hitachi) were gathered under an acceleration voltage of 15 kV after samples were gold sputter coated. Transmission Electron Microscopy (TEM) micrographs were obtained on a Tecnai T12 (Thermo-Fisher) electron microscope at an accelerating voltage of 120 kV. The transverse sections of samples for electron microscopy were cut *via* an Ultracut E ultramicrotome. Sections were 80 nm thick and supported on grids coated with a pioloform film.

2.3.2. Spectroscopy characterization

Bulk infrared spectra were acquired using a PerkinElmer Spectrum 100 FTIR spectrometer (Beaconsfield, UK). The spectrum range was 4000–600 cm^{-1}, and 16 scans were acquired and co-added for each measurement. Spectrum software was used for the collection and analysis of IR spectra.

To distinguish each phase from one another and thus to further understand the chemical distribution in the phase-separated domain in such ternary films, atomic force microscopy-infrared (AFM-IR) spectral measurements were performed on a NanoIR3 system (Bruker Nano Surfaces & Metrology, Santa Barbara, USA Cooperation) operating with top-down illumination and equipped with two pulsed tuneable lasers (Fast Spectra OPO and Fast Spectra QCL) to cover the wavenumber range from 3600 to 2700 cm^{-1} and 1800–800 cm^{-1}, respectively. The experimental configuration is shown schematically in Fig.S2 along with the measurement principle of the photothermal AFM-IR technique. In addition to the IR spectra, the AFM-IR provides IR images, the so-called chemical mapping, with which the individual components can be identified [32,33,36]. The ratio of AFM-IR maps at different wavelengths is often used for chemical analysis to cancel the possible nonchemical effects on the IR signal response such as the sample stiffness and different thermal expansion coefficients [37]. In this work, a contact cantilever was used for data acquisition, which was operated in contact AFM mode (resonance-enhanced AFM-IR mode). Scans were performed at wavelengths wavenumbers of 2932 cm^{-1}, 2802 cm^{-1}, 1512 cm^{-1}, and 1456 cm^{-1}; ratio images were created from the individual scans. The individual scans are put into ratio and the height images of the individual measurements are subtracted/correlated. All the images generated were subsequently analysed using Analysis Studio software (Anasys InstrumentsBruker Nano Surfaces and Metrology, Santa Barbara, CA, USA).

2.3.3. Properties measurements

Mechanical properties. Nanoindentation tests were performed using a Hysitron TI Premier nanoindentation with Berkovich diamond tip under load control at room temperature. Each composite sample was subject to one set of nanoindentation test. For each sample, at least five indents were performed at different domains on the surface. The loading rate and maximum loading were 500 nN/s and 5mN, respectively. The unloading rate was set equal to the loading rate. The loading time, holding time, unloading time, and maximum indentation force (P_{max}) are 10 s, 20 s, and 10 s for all testing samples. The separation distance

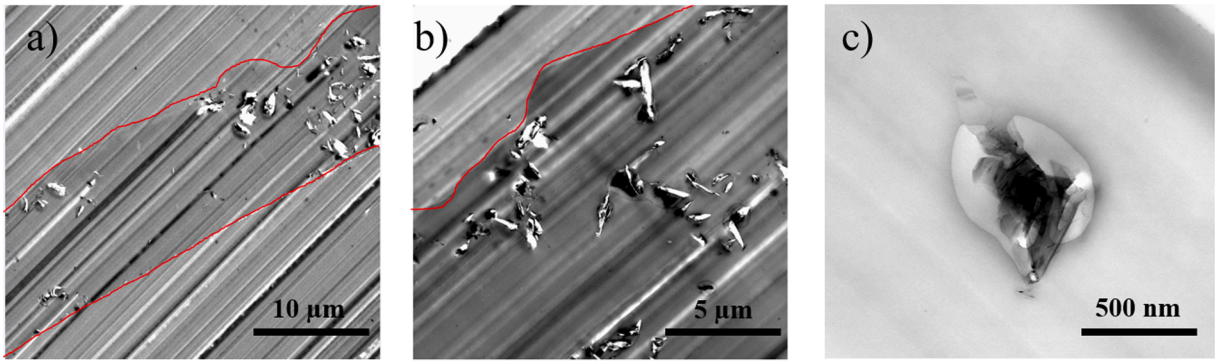

Fig. 2. TEM images (cross-section) of the phase-separated domain. Scale bars, 10 μm (a), 5 μm (b) and 500 nm (c). (Red line distinguishing the nanocomposite films with the underneath support film.) (For interpretation of the references to colour in this figure legend, the reader is referred to the web version of this article.)

between each nanoindentation point was 100 μm. The relative elastic modulus (Er) was obtained for each set of data of indented samples. Young's Modulus E was calculated from the following equations [38]:

$$\frac{1}{Er} = \frac{1-v^2}{E} - \frac{1-v_i^2}{E_i} \tag{1}$$

where E_i (1140 GPa) and ν_i (0.07) are the elastic moduli and Poisson's ratio of the diamond indenter [39], and $\nu = 0.34$ is the Poisson's ratio of the epoxy resin [40].

Thermal properties. Transient thermoreflectance (TTR) measurements were conducted to access the thermal conductivity of the thin composite films. The samples were coated with 145 nm of Au on a 10 nm Cr adhesion layer as a transducer. A 532 nm probe laser (spot size ~2 μm) was used to monitor the reflectivity, while a 355 nm nanosecond-pulsed pump laser (spot size ~85 μm) was used to periodically heat the sample surface [41]. The experimental configuration and principle of TTR measurement are described in Ref. [42]. The thermal conductivity of different samples was fitted by the properties of materials, as summarised in Table S1. Specific heat of the composite films was measured by using a Netzsch differential scanning calorimeter (DSC 204F1).

Scanning Probe Microscopy (SThM) measurements were carried out on a Nano-IR2 system (Bruker, Santa Barbara, CA, United States) *via* the SThM mode with a scan rate of 0.2 Hz per line, which is a mode where a special AFM tip is scanned across the sample surface in the contact mode by using a resistive thermal probe. As the tip changes temperature due to variations in the thermal conductivity or temperature of the sample in contact with the tip, the resistance of this element changes. This resistance change is monitored by the hardware using a Wheatstone bridge circuit and can be output to the controller to generate an image. The design and specific information about the bridge configuration are reported in Ref. [43]. Then the voltage applies to the resistive thermal probe, balances the Wheatstone bridge and measures a voltage that is characteristic of the resistance of the probe. Thus, the SThM image shows the change in output voltage for the two domains due to their differences in thermal conductivity. The electrical resistivity of the probe is 600 O and the heating voltage is 2 V.

Dielectric properties. The broadband frequency dielectric characteristics of the composites were measured using a Solartron SI 1260 impedance analyzer (Advanced Measurement Technology, Inc, UK) in a frequency range of 10^2 to10^5 Hz. All the samples have a layer of silver coated on both surfaces to serve as electrodes. The samples were considered as plane capacitors and described by parallel resistor–capacitor (RC) circuit systems. The complex dielectric constant (ε^*) was calculated as follows:

$$\varepsilon^* = \varepsilon^{'} - j\varepsilon^{''} \tag{2}$$

where $\varepsilon^{'}$ and $\varepsilon^{''}$ correspond to the real and imaginary parts of the complex dielectric constant, respectively. $\omega = 2\pi f$ is the angular frequency, and the dielectric loss tangent (tan δ) was defined as

$$tan\delta = \frac{\varepsilon^{''}}{\varepsilon^{'}} \tag{3}$$

3. Results and discussion

3.1. Self-assembled microdomains

Fig. 1 schematically depicts a facile procedure involving the chemical structures depicted for fabricating the phase-separated structure with localization of A-GNPs in the continuous domain. The material prepared is a very simple and liquid processable multicomponent commercial epoxy blend containing A-GNPs as the reinforcing particles. Normally, a nanocomposite with well-dispersed nanosheets in the epoxy matrix would be fabricated (as shown in Fig. 1a), abbreviated as Homogeneous. Fig. 1b shows the corresponding distribution of nanosheets in the epoxy matrix. The resin blend containing AEPIP (Fig. 1c) formed a bi-continuous phase-separated microdomain with a width in the range of 10–40 μm (Fig. 1d), abbreviated as Separated. AFM images (Fig. 1.e) and SEM image (Fig.S3) demonstrate the topology and morphology of the phase-separated microstructure that is constructed in the epoxy nanocomposite film containing amine-functionalized graphene nanoparticles (A-GNPs). The smooth surface is epoxy-rich, while the domain with the rippled surface is characterized by the presence of graphene nanosheets, which suggests that during the polymerization the nanosheets aggregate to form a dense domain. Finally, a 3D structured composite film with a thickness of 20 to 30 μm was fabricated (Fig. 1.f). It is worth noting that the irregular thickness observed in these films is not a function of the spin coating process but is due to the mechanism of morphology development in the nanocomposite films. It arises from an interrelated series of steps involving polymerisation kinetics, miscibility, and nanomaterial assembly. A full discussion of the mechanism would be the subject of a subsequent manuscript.

The morphology of the phase-separated domains was analysed by TEM, revealing the fine details of the nanosheets embedded in the matrix (Fig. 2). It is clear that a resin domain and graphene domain are produced; the latter containing aggregated nanosheets. In the graphene domain, some individual nanosheets (which are transparent, being formed by only a few layers of graphene) could be seen, which indicates that the graphene domain is not a big agglomeration of nanosheets but constructed by a numbers of individually dispersed graphene nanosheets. This might be due to the fact that a secondary phase separation would normally present in the microdomain [44]. It should be noted that a large agglomeration of nanoparticles would suppress the excellent properties of nanofillers, while the graphene domain that contains high-performance resin reinforced with a high amount of individual graphene might offer excellent multifunctional properties [13].

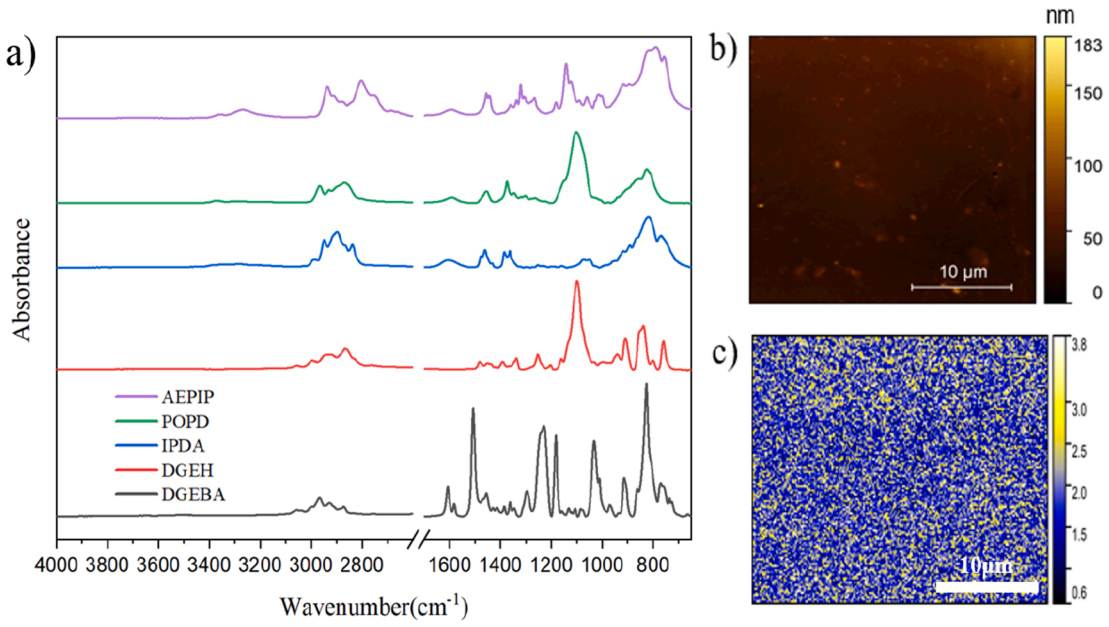

Fig. 3. a) FTIR spectrum of each component, b) AFM image and c) Chemical map of the Homogeneous blend (obtained by constructing a ratio of IR absorption images at 1456 cm^{-1}/1512 cm^{-1}) (Scale bar: 10 μm).

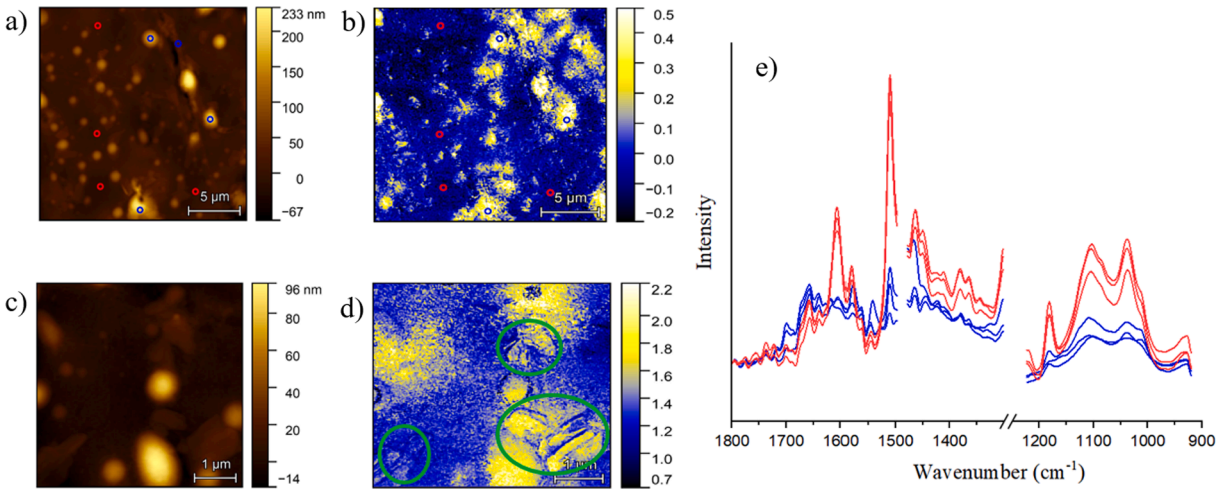

Fig. 4. a, c) AFM image and b, d) Chemical map (ratio of IR absorption images at 1456 cm^{-1}/1512 cm^{-1}) of the Separated blend, e) AFM-IR absorption spectra obtained at locations indicated in a). (Green circles highlight the graphene dispersed in the blend.) (For interpretation of the references to colour in this figure legend, the reader is referred to the web version of this article.)

3.2. *Chemical distribution characterization*

Selective localization of nanofillers in phase-separated structures in TS/TS systems is rarely reported and the mechanism remains largely unknown due to the complicated copolymerization between different components during the curing process. Therefore, the photothermal AFM-IR technique, a rapidly emerging technique that accesses a spatial resolution compositional mapping on the nanoscale, was used to investigate the chemical distribution of different samples, which might provide essential evidence for studying the mechanism of the phase behaviour of this multi-component blend. Bulk IR spectra were obtained *via* conventional FTIR spectroscopy for identifying the chemical structure of each component before accessing the chemical differences of each domain by AFM-IR. As seen in Fig. 3a, although component B and C are both amine reagents, a significant difference could be discerned in the region of 2710–2810 cm^{-1}, which is assigned to the stretching vibration of the C-H bond of the N-CH_2 group in AEPIP. As the epoxy resin is mainly formed by the DGEBA, even though there is no obvious IR peak for identifying the DEGH and hardeners, the distinct vibration of the aromatic ring in the 1512 cm^{-1} of DGEBA can be utilized as the spectral signature of the epoxy resin in the blend.

Fig. 3b presents an AFM height image of the RM135/RS-MH137 (Homogeneous) blend with A-GNPs. A smooth surface with some small features (nanofillers) could be observed, which reveals that the topology of the blend with homogeneously dispersed A-GNP is completely different from the one with a phase-separated structure. There are no obvious phase behaviour could be seen in this blend, and the chemical map constructed by the ratio of IR absorption images at 1456 cm^{-1} (C-H bending) /1512 cm^{-1} confirming that no heterogeneous chemical structure could be discerned at the microscale. However, chemical analysis in sub-micro to nanoscale should be accessed, as many researchers have previously reported that phase-separated nanodomains were constructed in the binary polymer blends, such as block-copolymer/TS [45], rubber/TS [46] as well as TS/TS [19,47] blends.

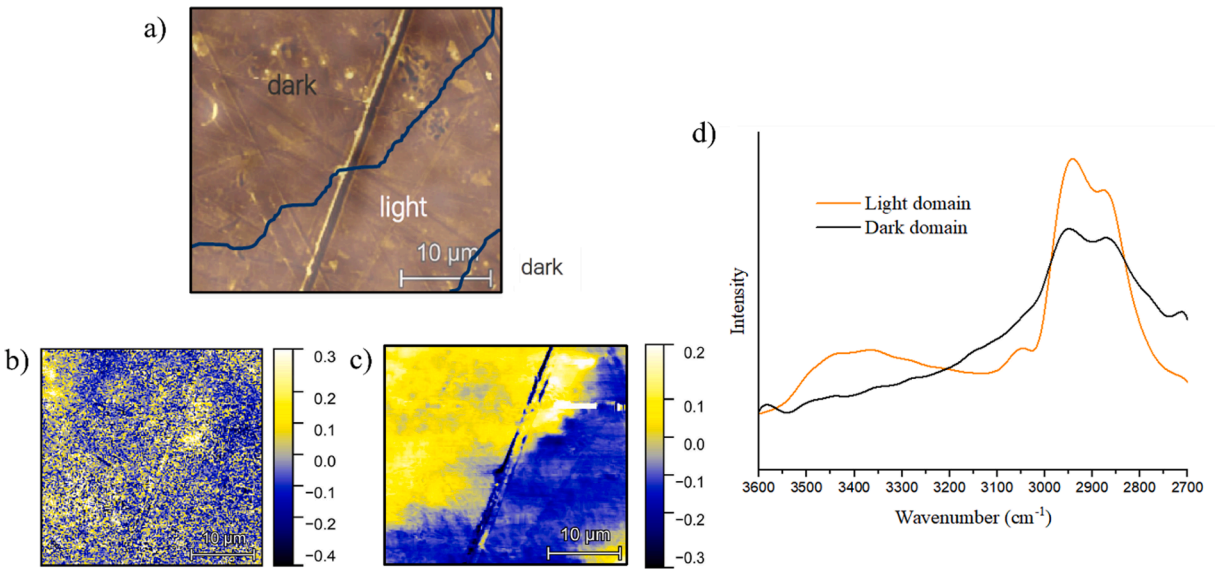

Fig. 5. a) Optical image and Chemical map of the Separated blend (obtained by constructing a ratio of IR absorption images at b) 1456 cm^{-1}/1512 cm^{-1} and c) 2932 cm^{-1}/2800 cm^{-1}, d) AFM-IR absorption spectra obtained different domains.

Fig. 4 depicts the chemical differences of the Homogeneous blend that are visible at the sub-micron level. In addition to the heterogeneous chemical distribution that is evident, in Fig. 4e, the recorded AFM-IR spectra of the colour-coded locations highlight that there are epoxy-rich (blue) and curing agent-rich (yellow) domains within the blend at the sub-micron scale. It should be noted that the AFM-IR spectrum of each domain is consistent, which means that with photothermal AFM-IR it is possible to map unambiguously the distribution of the different chemical components on the nanoscale. In Fig. 4d, the high-resolution chemical map clearly shows the dimensions of each domain and it appears that the epoxy domain is the continuous domain with curing agent-richinclusions; similar phase behaviour of epoxy blends containing hard and soft phases has previously been reported [47,48]. In addition, the random distribution of graphene highlighted in Fig. 4d implies that the selective localization of A-GNP would not be induced by the formation of this heterogeneous nanostructure. This could be because the dimension of the nanofiller is bigger than the phase-separated domains or the domains are too small, and thus a large amount of attraction points disturbs the localization of the nanofillers. A similar phenomenon was observed by Wang *et al.* [49], where the phase-separated nanodomains in carboxy-terminated butadiene acrylonitrile/epoxy blends did not influence the localization of graphene.

In this work, A-GNP has been identified in the phase-separated microstructure and, as shown in Fig. 5a, the dark and light domains are clearly highlighted. The Homogeneous blend displays distinct epoxy and hardener-rich domains whereas the epoxy blend containing AEPIP (Component C) shows a homogeneous distribution of epoxy and curing agents (Fig. 5b). Conversely, when the chemical map turns to the ratio of 2802 cm^{-1}/ 2932 cm^{-1} (C-H stretching of asymmetric methylene), it can be seen that the graphene (dark) domain is displaying much stronger absorptions than the resin (light) domain at 2802 cm^{-1}. Comparing the AFM-IR spectra to FTIR reference spectra of each component (Fig. 3a), it could be confirmed that the graphene domains contain more AEPIP than the resin domain. This indicates that the nanosheets are selectively located in the domain with a higher amount of AEPIP, meaning that AEPIP is the driving force behind the formation of this phase-separated

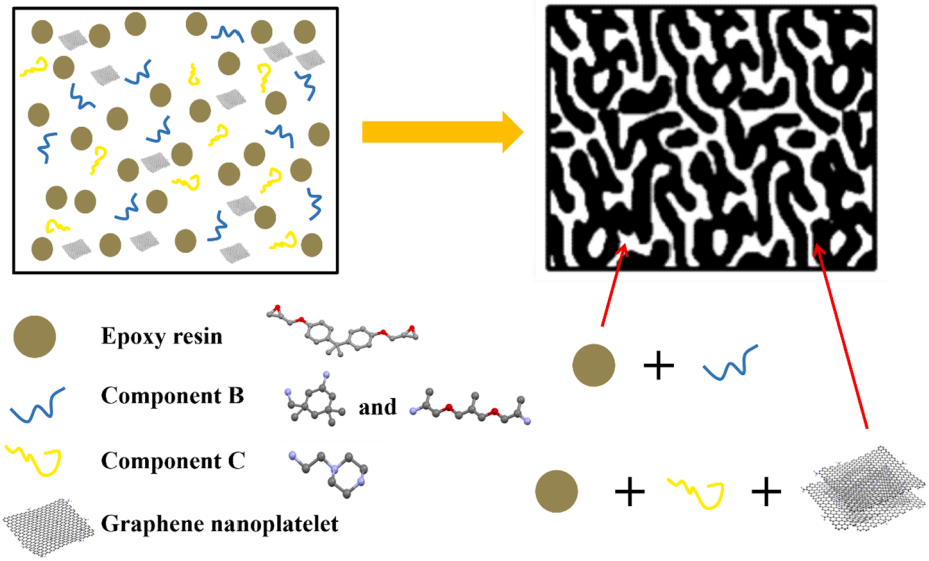

Fig. 6. Component distribution in the phase-separated structure.

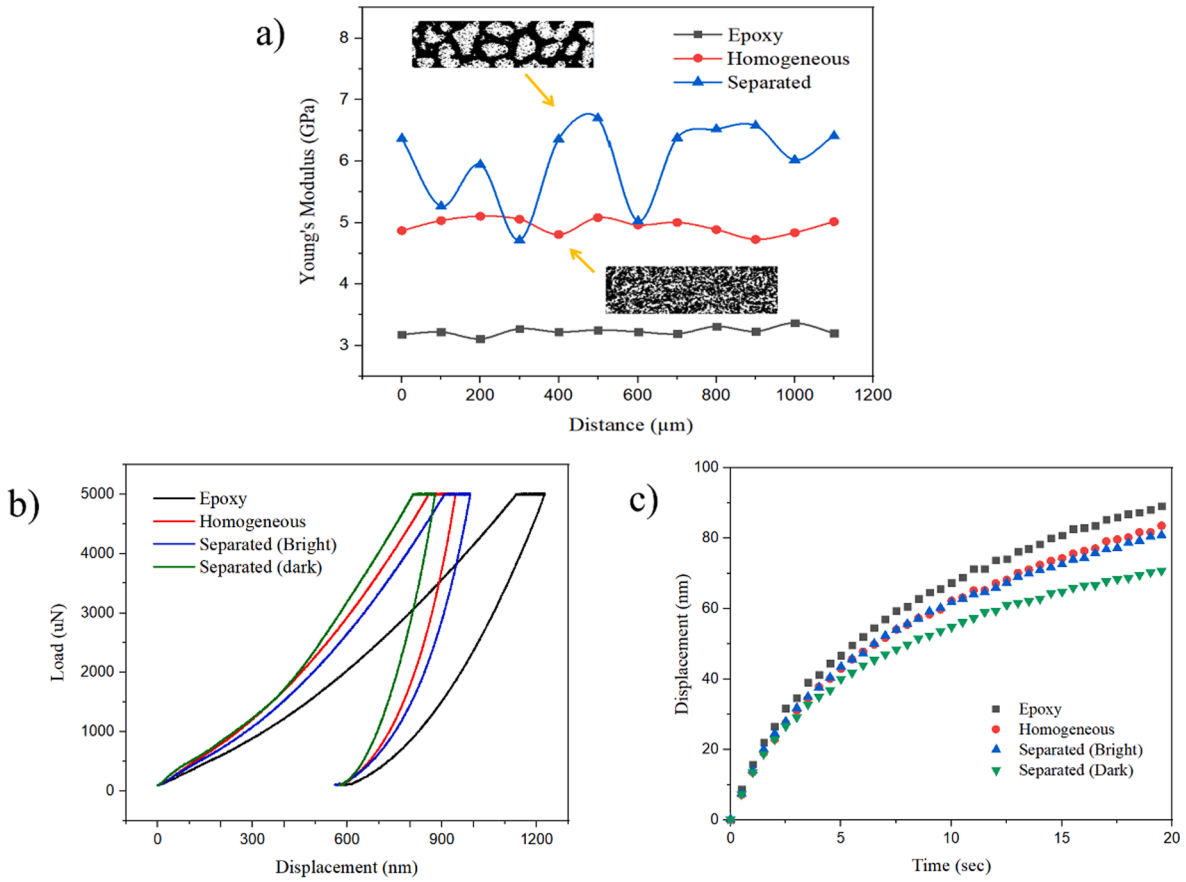

Fig. 7. a) Modulus variations along the indentation array. **b)** Representative load–displacement curves derived from nanoindentation tests. **c)** Nanoindentation creep deformation at a maximum load of 5000 μN.

graphene domain. It is therefore confirmed that the the graphene nanosheets migrate to the AEPIP-rich region and aggregate to form a dense column through the thickness (Fig. 1f). Furthermore, as shown in Fig. 5d, a significant chemical contrast could be seen between the dark and light domain in the region of 3300 to 3500 cm^{-1}, which is assigned to the N-H stretching of the primary amine and the O-H stretching from the hydroxyl groups formed by the curing reaction of epoxy and hardeners. This implies that the epoxy (light) domain contains more primary amine groups and epoxy oligomers would be extruded by the aggregation of the graphene domain.

This high-resolution AFM-IR mapping allows the composition of each domain to be identified, which provides critical indications for investigating the mechanism of selective localization in phase-separated structures in thermoset blends. The composition distribution is schematically shown in Fig. 6, the dark domain is constructed by graphene nanosheets, AEPIP and epoxy resin, while the light domain is formed by the epoxy resin with IDPA and POP. Most importantly, it is worth noting that the addition of graphene could make the unexpected phase separation by incorporating AEPIP in a commercial multi-component become visible without the necessity for an etching process; it is well known that the phase separation extent in TS/TS blending systems is normally very low and the contrast between two phases is too ambiguous to be observed. This provides an effective way for investigating the morphological evolutions of phase separation in TS systems, which is an important issue to understand the roles of each component in the phase separation and realize the preparation of TS/TS blends with different selective localized nanofiller in a controllable manner [50]. Work is continuing to conduct further exploration for having a comprehensive understanding of this phase behaviour.

3.3. Properties

The observed phase-separated structure constructed with well-dispersed nanosheets, was expected to lead to a microstructure with superior mechanical and thermal properties. Consequently, nanoindentation was used to measure the Young's modulus along the bi-continuous microdomain. As shown in Fig. 7a, the unmodified epoxy resin displays the lowest modulus (3.2 GPa) and the average modulus of composite film with homogeneous dispersed A-GNP increases to 4.9 GPa; this is attributed to the introduction of graphene nanosheets. The physical interlocking, covalent adhesion, and presence of high-density bonds between A-GNP and the matrix facilitate rapid transfer or absorption of energy, leading to a significant improvement in mechanical performance [51]. Most importantly, it should be noted that the samples that do not display the phase-separated microstructure possess relatively uniform modulus and hardness values along the indentation array, which is consistent with the composition distribution and polymerization observed previously *via* AFM-IR. In contrast, the samples displaying the bi-continuous phase-separated morphology, show considerable heterogeneity in modulus and hardness values in different regions of the indentation array. Even though this specific phase-separated microstructure shows fluctuations in the value of mechanical properties, the average value is much higher than the other samples.

The loading displacement curve and the displacement–time plot are illustrated in Fig. 7b and c, respectively, to further study the mechanical behaviour of the composites film with different phase morphology. With the incorporation of A-GNP, the load–displacement curve is shifted to the leftdue to the growth in stiffness of the nanocomposite film. Thus, the elastic modulus will increase with the increase in the required load to penetrate the surface. The total indentation depth of the dark (A-GNP-

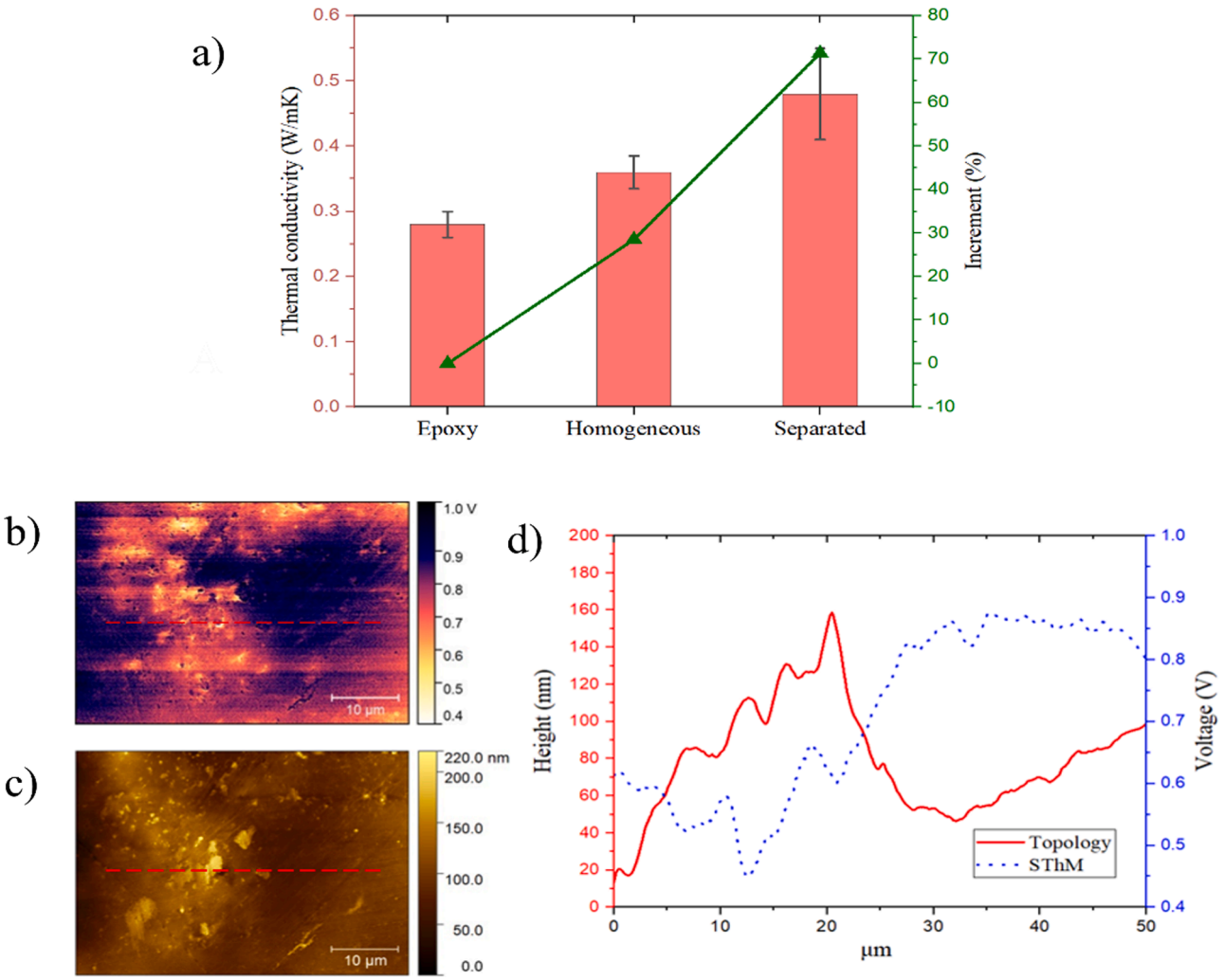

Fig. 8. TTR and SThM measurement of the epoxy/A-GNPs nanocomposites with phase-separated structure, (a) thermal conductivity, (b) SThM mapping, (c) corresponding AFM mapping (d) plot of topology and SThM variation along the array.

rich) domain decreased by about 27% compared with the unreinforced epoxy film and by about 9% compared with the epoxy film reinforced with homogeneous dispersed A-GNP. These results demonstrate that the incorporation of A-GNP improves the load bearing capacity of the epoxy resin, and the dark domain presents an additional improvement due to the highly dense graphene microstructure. Similarly, as shown in Fig. 7c, there is a remarkable increase in the creep resistance, due to the confinement effect of the highly elastic graphene sheets that can effectively prevent the deformation of the epoxy network and improve the load transfer mechanism.

The mechanical properties of the different samples are summarized in Table.S2, from which it can be seen that the modulus of the resin-rich domain displays a similar value to the homogeneous sample and the graphene-rich domain reached 6.3 GPa, exhibiting a significant enhancement (97%) when compared to the unreinforced epoxy resin. In this particular case, in addition to the outstanding mechanical performance of graphene sheets, the distinct A-GNP domain displays a superior modulus thanks to its highly dense A-GNP microstructure. Surprisingly, the samples containing the resin-rich domains display mechanical properties that are similar to the sample reinforced with homogeneously dispersed nanosheets, which might be due to the reinforcement of the sheets that remain in the light domain and the synergistic confinement effect of the continuous graphene channels.

The thermal conductivity of the epoxy/A-GNP nanocomposites was measured *via* TTR, which is a powerful technique normally used to measure the thermal conductivity of the materials used in the semiconductor industry [41,42]. As shown in Fig. 8, the nanocomposite film containing homogeneously dispersed A-GNPs shows an enhancement of only 30% compared with the unmodified epoxy film. It has been reported that the covalent bonds between A-GNP and epoxy provide enhanced interface thermal conductance and vibrational coupling of phonons in the epoxy matrix, thus presenting an ideal choice for enhancing thermal conductivity of epoxy-based nanocomposite [11]. However, the perfectly dispersed graphene sheets decreased the possibility of the interconnection of the graphene sheets, decreasing the contact interface and thus increasing phonon scattering, which are the major obstacles to the overall thermal conductivity. This could be confirmed by the significant enhancement (72%) of thermal conductivity that was observed for the nanocomposite film with a continuous graphene domain, which implies that the self-constructed graphene microstructure results in a decreased phonon scattering. In addition, the variations in the thermal conductivity between different regions in the phase-separated sample might be because the laser spot size (85 μm) is larger than the width of the graphene channel, and thus the area fraction of the dark and light domain was various between each measurement.

Hence, to further correlate the local thermal properties directly with the microstructural heterogeneity features, SThM measurement was carried out to accomplish the microscopic thermoelectric conversion down to the submicron level. As shown in Fig. 8b, when the probe scans different phases, heat transfers from the probe to the sample, resulting in

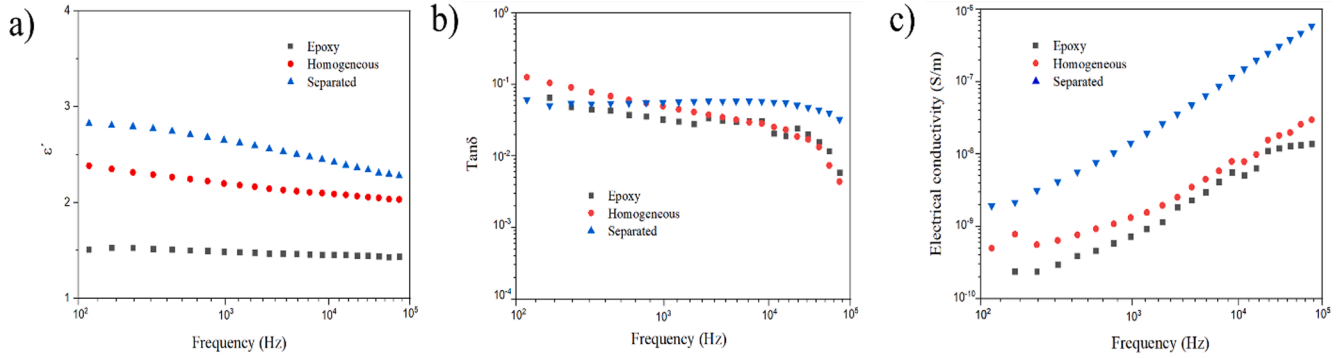

Fig. 9. Dielectric properties of the epoxy/A-GNPs nanocomposites.

drops in its temperature and resistance, and thus a voltage drop between nodes A and B of the Wheatstone bridge. The phase with the lower sample thermal conductivity has a lower heat loss and thus a lower bridge voltage difference (Fig. 8b). The corresponding SThM image displays the hotter areas as dark because the greater the probe temperature, the higher the resistance and the output voltage, resulting in a lower conductivity of those regions. Consequently, the greater voltage difference observed for the graphene domain indicates a higher sample thermal conductivity (Fig. 8d), implying that it is possible to image the local thermal conductivity variation of a phase-separated structure with a self-assembled graphene domain based on the bridge voltage *via* SThM. However, even though the flattest region was chosen for measurement, the SThM images obtained with any AFM based scanning thermal technique are not quantitative due to the inevitable topographical effects [52]. The clear contrast between graphene-rich and resin-rich domains emphasized the importance of constructing a continuous conductive network to overcome the obstacle of enhancing the thermal conductivity of epoxy-based composites. Thus, TTR is presented as a powerful technique to access the thermal conductivity of the sample, while the function of the SThM images is to provide image contrast based on the correlated local thermal properties of the phases or components in micro-nano structured materials, which can be used to guide the design and optimization of thermoelectric materials with enhanced performance.

Fig. 9 displays the frequency-dependent dielectric properties of the epoxy/A-GNPs nanocomposites, from which it is apparent that both the dielectric constant and dielectric loss tangent of the nanocomposites are slightly higher than those of the unmodified epoxy resin over the whole frequency range. This is closely associated with the electrical conductivity of the epoxy composites [53,54].

Compared to the pristine graphene sheets, A-GNPs exhibit lower electrical conductivity, which can be explained by the fact that the amine functionalization produces large amounts of sp^3 hybridized carbon atoms due to the formation of the C-N bond [55], this results in a reduction in the conductivity due to the loss of delocalization. Even though the nanocomposite film with a continuous graphene domain presents a higher conductivity, the enhancement is negligible as the conductivity is still lower than the antistatic criterion of 10^{-6} S/m, which means that the nanocomposite film with phase-structured graphene domains is still an insulator. Additionally, a subtle difference in the low dielectric loss between different samples could be observed, which might be because the mobility of the charge carriers is inhibited by the secondary resin-rich microstructure within the graphene domain (Fig. 2). These results imply the potential practical application of this material, as the material with low dielectric loss can minimize heat generated under an electric field, which can finally prevent the ruin of the performance, and thus improve the lifetime and reliabilities of electric devices and apparatus [2].

4. Conclusions

In this work, it has been demonstrated that nanoparticles could be successfully located in a bi-continuous microstructure from an entirely miscible blend. SEM, TEM, and AFM techniques were employed to exhibit this specialist phase morphology, confirming the construction of a dense graphene domain within a bi-continuous phase structure. Nanoindentation measurement shows that the graphene domain has a dramatic (97%) increase in Young's modulus, meanwhile, the mechanical properties of the epoxy domain also exhibit a slight increase when compared to the unreinforced epoxy film. Similarly, TTR measurement depicts that the thermal conductivity of composite film with continuous graphene domains shows an enhancement of 72%. In order to access the local thermal properties of different domains and their interfaces, SThM measurement was employed and obvious contrast between each domain could be discerned. Hence, a dielectric polymer composite with excellent thermal conductivity and mechanical properties was fabricated, which is very promising for microelectronic packaging and thermal management application in new energy systems such as light-emitting diodes (LEDs) and solar cells. Most importantly, our investigation of chemical distribution *via* the AFM-IR technique provides consolidated evidence for confirming the localization of nanofillers in self-assembled microstructure is associated with the chemical difference in various phases, which provides essential clues to unlock the potential application of epoxy-based nanocomposites.

CRediT authorship contribution statement

Suihua He: Conceptualization, Methodology, Investigation, Writing – original draft. **Hartmut Stadler:** Methodology. **Xuankai Huang:** Methodology. **Xiang Zheng:** Methodology. **Guanjie Yuan:** Methodology. **Martin Kuball:** Methodology. **Miriam Unger:** Methodology. **Carwyn Ward:** Supervision, Conceptualization, Writing – review & editing. **Ian Hamerton:** Supervision, Conceptualization, Writing – review & editing.

Declaration of Competing Interest

The authors declare that they have no known competing financial interests or personal relationships that could have appeared to influence the work reported in this paper.

Acknowledgements

S.H. is supported through China Scholarship Council/University of Bristol (CSC-UOB) Joint Research Scholarship and wishes to thank the Faculty of Engineering Research Pump Priming Fund (UOB). S.H., C.W., and I.H., would like to acknowledge the support of Bruker Nano Surfaces & Metrology, and the Henry Royce Institute through the Royce PhD Equipment Access Scheme enabling access to imaging and

characterization facilities at Royce@Sheffield and Royce@Manchester; EPSRC Grant Number EP/R00661X/1. S.H., C.W., and I.H., also wish to thank Dr Germinal Margo and Dr Annela Seddon for approval for the access to the spin coater and useful discussions.

Appendix A. Supplementary data

Supplementary data to this article can be found online at https://doi.org/10.1016/j.apsusc.2022.154925.

References

[1] X. Huang, T. Iizuka, P. Jiang, Y. Ohki, T. Tanaka, Role of interface on the thermal conductivity of highly filled dielectric epoxy/AlN composites, J. Phys. Chem. C 116 (25) (2012) 13629–13639.
[2] X. Huang, C. Zhi, P. Jiang, D. Golberg, Y. Bando, T. Tanaka, Polyhedral oligosilsesquioxane-modified boron nitride nanotube based epoxy nanocomposites: an ideal dielectric material with high thermal conductivity, Adv. Funct. Mater. 23 (14) (2013) 1824–1831.
[3] H. Zeng, C. Zhi, Z. Zhang, X. Wei, X. Wang, W. Guo, Y. Bando, D. Golberg, "White graphenes": boron nitride nanoribbons via boron nitride nanotube unwrapping, Nano Lett. 10 (12) (2010) 5049–5055.
[4] Z. Wang, J. Luo, G.L. Zhao, Dielectric and microwave attenuation properties of graphene nanoplatelet–epoxy composites, AIP Adv. 4 (1) (2014), 017139.
[5] X.-Y. Qi, D. Yan, Z. Jiang, Y.-K. Cao, Z.-Z. Yu, F. Yavari, N. Koratkar, Enhanced electrical conductivity in polystyrene nanocomposites at ultra-low graphene content, ACS Appl. Mater. Interfaces 3 (8) (2011) 3130–3133.
[6] L. Chen, P. Zhao, H. Xie, W. Yu, Thermal properties of epoxy resin based thermal interfacial materials by filling Ag nanoparticle-decorated graphene nanosheets, Compos. Sci. Technol. 125 (2016) 17–21.
[7] A. Nouri-Borujerdi, S. Kazemi-Ranjbar, Thermal and electrical conductivity of a graphene-based hybrid filler epoxy composite, J. Mater. Sci. 56 (27) (2021) 15151–15161.
[8] S. He, J. Zhang, X. Xiao, X. Hong, Y. Lai, Investigation of the conductive network formation of polypropylene/graphene nanoplatelets composites for different platelet sizes, J. Mater. Sci. 52 (22) (2017) 13103–13119.
[9] S. Stankovich, D.A. Dikin, G.H. Dommett, K.M. Kohlhaas, E.J. Zimney, E.A. Stach, R.D. Piner, S.T. Nguyen, R.S. Ruoff, Graphene-based composite materials, Nature 442 (7100) (2006) 282–286.
[10] S. Zhu, R. Shi, M. Qu, J. Zhou, C. Ye, L. Zhang, H. Cao, D. Ge, Q. Chen, Simultaneously improved mechanical and electromagnetic interference shielding properties of carbon fiber fabrics/epoxy composites via interface engineering, Compos. Sci. Technol. 207 (2021), 108696.
[11] X. Shen, Z. Wang, Y. Wu, X. Liu, J.-K. Kim, Effect of functionalization on thermal conductivities of graphene/epoxy composites, Carbon 108 (2016) 412–422.
[12] B. Nazari, Z. Ranjbar, R.n.R. Hashjin, A. Rezvani Moghaddam, G. Momen, B. Ranjbar, Dispersing graphene in aqueous media: Investigating the effect of different surfactants, Colloids Surf. A: Physicochem. Eng. Aspects 582 (2019).
[13] S. He, J. Zhang, X. Xiao, Y. Lai, A. Chen, Z. Zhang, Study on the morphology development and dispersion mechanism of polypropylene/graphene nanoplatelets composites for different shear field, Compos. Sci. Technol. 153 (2017) 209–221.
[14] X. Wang, W. Li, Z. Zhang, K. Chen, W. Gan, Selective localization of multi-walled carbon nanotubes in epoxy/polyetherimide system and properties of the conductive composites, J. Appl. Polym. Sci. 136 (35) (2019).
[15] Y. Zhang, Y. Shen, K. Shi, T. Wang, E. Harkin-Jones, Constructing a filler network for thermal conductivity enhancement in epoxy composites via reaction-induced phase separation, Compos. A Appl. Sci. Manuf. 110 (2018) 62–69.
[16] X. Jin, W. Li, Y. Liu, W. Gan, Self-constructing thermal conductive filler network via reaction-induced phase separation in BNNSs/epoxy/polyetherimide composites, Composites Part A: Appl. Sci. Manuf. 130 (2020).
[17] M. Nofar, R. Salehiyan, S.S. Ray, Influence of nanoparticles and their selective localization on the structure and properties of polylactide-based blend nanocomposites, Compos. B Eng. 215 (2021).
[18] J. Kratz, T. Mesogitis, A.A. Skordos, I. Hamerton, I.K. Partridge, Developing cure kinetics models for interleaf particle toughened epoxies, (2016).
[19] X. Li, X. Luo, Y. Gu, A novel benzoxazine/cyanate ester blend with sea-island phase structures, PCCP 17 (29) (2015) 19255–19260.
[20] Z. Wang, L. Li, Y. Fu, Y. Miao, Y. Gu, Reaction-induced phase separation in benzoxazine/bismaleimide/imidazole blend: Effects of different chemical structures on phase morphology, Mater. Des. 107 (2016) 230–237.
[21] Z. Wang, Q. Ran, R. Zhu, Y. Gu, A novel benzoxazine/bismaleimide blend resulting in bi-continuous phase separated morphology, RSC Adv. 3 (5) (2013) 1350–1353.
[22] Z. Wang, Q. Ran, R. Zhu, Y. Gu, Reaction-induced phase separation in a bisphenol A-aniline benzoxazine-N, N'-(2,2,4-trimethylhexane-1,6-diyl)bis(maleimide)-imidazole blend: the effect of changing the concentration on morphology, Phys Chem Chem Phys 16 (11) (2014) 5326–5332.
[23] Z. Wang, N. Cao, Y. Miao, Y. Gu, Influence of curing sequence on phase structure and properties of bisphenol A-aniline benzoxazine/N, N′-(2,2,4-trimethylhexane-1,6-diyl) bis (maleimide)/imidazole blend, J. Appl. Polym. Sci. 133 (14) (2016) n/a-n/a.
[24] P. Zhao, Q. Zhou, Y.Y. Deng, R.Q. Zhu, Y. Gu, Reaction induced phase separation in thermosetting/thermosetting blends: effects of imidazole content on the phase separation of benzoxazine/epoxy blends, RSC Adv. 4 (106) (2014) 61634–61642.
[25] J. Yue, L. He, P. Zhao, Y. Gu, Engineering benzoxazine/epoxy/imidazole blends with controllable microphase structures for toughness improvement, ACS Appl. Polym. Mater. 2 (8) (2020) 3458–3464.
[26] J. Huang, N. Li, L. Xiao, H. Liu, Y. Wang, J. Chen, X. Nie, Y. Zhu, Fabrication of a highly tough, strong, and stiff carbon nanotube/epoxy conductive composite with an ultralow percolation threshold via self-assembly, J. Mater. Chem. A 7 (26) (2019) 15731–15740.
[27] A. Vital, M. Vayer, T. Tillocher, R. Dussart, M. Boufnichel, C. Sinturel, Morphology control in thin films of PS:PLA homopolymer blends by dip-coating deposition, Appl. Surf. Sci. 393 (2017) 127–133.
[28] A. Vital, M. Vayer, C. Sinturel, T. Tillocher, P. Lefaucheux, R. Dussart, Polymer masks for structured surface and plasma etching, Appl. Surf. Sci. 332 (2015) 237–246.
[29] R. Yu, S. Zheng, Morphological Transition from Spherical to Lamellar Nanophases in Epoxy Thermosets Containing Poly(ethylene oxide)-block-poly(ε-caprolactone)-block-polystyrene Triblock Copolymer by Hardeners, Macromolecules 44 (21) (2011) 8546–8557.
[30] A. Dazzi, C.B. Prater, AFM-IR: Technology and Applications in Nanoscale Infrared Spectroscopy and Chemical Imaging, Chem Rev 117 (7) (2017) 5146–5173.
[31] B. Lahiri, G. Holland, A. Centrone, Chemical imaging beyond the diffraction limit: experimental validation of the PTIR technique, Small 9 (3) (2013) 439–445.
[32] S. Morsch, Y. Liu, S.B. Lyon, S.R. Gibbon, Insights into Epoxy Network Nanostructural Heterogeneity Using AFM-IR, ACS Appl Mater Interfaces 8 (1) (2016) 959–966.
[33] Q. Zhu, R. Zhou, J. Liu, J. Sun, Q. Wang, Recent Progress on the Characterization of Cellulose Nanomaterials by Nanoscale Infrared Spectroscopy, Nanomaterials (Basel) 11(5) (2021).
[34] J. Cheng, Z. Zhong, Y. Lin, Z. Su, C. Zhang, X. Zhang, Miscibility of isotactic poly(1-butene)/isotactic polypropylene blends studied by atomic force Microscopy−Infrared, Polymer 239 (2022).
[35] S. He, P. Bouzy, N. Stone, C. Ward, I. Hamerton, Analysis of the Chemical Distribution of Self-Assembled Microdomains with the Selective Localization of Amine-Functionalized Graphene Nanoplatelets by Optical Photothermal Infrared Microspectroscopy, Anal Chem 94 (34) (2022) 11848–11855.
[36] S. Morsch, P.D. Bastidas, Simon M. Rowland, AFM-IR insights into the chemistry of interfacial tracking, J. Mater. Chem. A 5(46) (2017) 24508-24517.
[37] D.E. Barlow, J.C. Biffinger, A.L. Cockrell-Zugell, M. Lo, K. Kjoller, D. Cook, W. K. Lee, P.E. Pehrsson, W.J. Crookes-Goodson, C.-S. Hung, The importance of correcting for variable probe–sample interactions in AFM-IR spectroscopy: AFM-IR of dried bacteria on a polyurethane film, Analyst 141 (16) (2016) 4848–4854.
[38] R. Poveda, N. Gupta, M. Porfiri, Poisson's ratio of hollow particle filled composites, Mater. Lett. 64 (21) (2010) 2360–2362.
[39] W.C. Oliver, G.M. Pharr, An improved technique for determining hardness and elastic modulus using load and displacement sensing indentation experiments, J. Mater. Res. 7 (6) (1992) 1564–1583.
[40] J. Cho, J. Luo, I. Daniel, Mechanical characterization of graphite/epoxy nanocomposites by multi-scale analysis, Compos. Sci. Technol. 67 (11–12) (2007) 2399–2407.
[41] C. Yuan, J.W. Pomeroy, M. Kuball, Above bandgap thermoreflectance for non-invasive thermal characterization of GaN-based wafers, Appl. Phys. Lett. 113 (10) (2018), 102101.
[42] D.E. Field, J.A. Cuenca, M. Smith, S.M. Fairclough, F.C. Massabuau, J.W. Pomeroy, O. Williams, R.A. Oliver, I. Thayne, M. Kuball, Crystalline Interlayers for Reducing the Effective Thermal Boundary Resistance in GaN-on-Diamond, ACS Appl Mater Interfaces (2020).
[43] M. Chirtoc, X. Filip, J. Henry, J. Antoniow, I. Chirtoc, D. Dietzel, R. Meckenstock, J. Pelzl, Thermal probe self-calibration in ac scanning thermal microscopy, Superlattices and Microstructures 35 (3–6) (2004) 305–314.
[44] K.A. Masser, E.D. Bain, F.L. Beyer, A.M. Savage, H.Y. Jian, J.L. Lenhart, Influence of nano-scale morphology on impact toughness of epoxy blends, Polymer 103 (2016) 337–346.
[45] S.M. George, D. Puglia, J.M. Kenny, J. Parameswaranpillai, S. Thomas, Reaction-Induced Phase Separation and Thermomechanical Properties in Epoxidized Styrene-block-butadiene-block-styrene Triblock Copolymer Modified Epoxy/DDM System, Ind. Eng. Chem. Res. 53 (17) (2014) 6941–6950.
[46] S.C. Leguizamon, J. Powers, J. Ahn, S. Dickens, S. Lee, B.H. Jones, Polymerization-Induced Phase Separation in Rubber-Toughened Amine-Cured Epoxy Resins: Tuning Morphology from the Nano- to Macro-scale, Macromolecules 54 (17) (2021) 7796–7807.
[47] S. Chen, L. Yuan, Z. Wang, A. Gu, G. Liang, Self-constructed nanodomain structure in thermosetting blend based on the dynamic reactions of cyanate ester and epoxy resins and its related property, Compos. B Eng. 177 (2019).
[48] K.A. Masser, E.D. Bain, F.L. Beyer, A.M. Savage, J.H. Yu, J.L. Lenhart, Influence of nano-scale morphology on impact toughness of epoxy blends, Polymer 103 (2016) 337–346.
[49] F. Wang, L.T. Drzal, Y. Qin, Z. Huang, Enhancement of fracture toughness, mechanical and thermal properties of rubber/epoxy composites by incorporation of graphene nanoplatelets, Compos. A Appl. Sci. Manuf. 87 (2016) 10–22.
[50] J. Yue, H. Wang, Q. Zhou, P. Zhao, Reaction-Induced Phase Separation and Morphology Evolution of Benzoxazine/Epoxy/Imidazole Ternary Blends, Polymers (Basel) 13 (17) (2021).

[51] Y. Chen, D. Li, W. Yang, C. Xiao, M. Wei, Effects of different amine-functionalized graphene on the mechanical, thermal, and tribological properties of polyimide nanocomposites synthesized by in situ polymerization, Polymer 140 (2018) 56–72.
[52] M.J. Pereira, J.S. Amaral, N.J. Silva, V.S. Amaral, Nano-localized thermal analysis and mapping of surface and sub-surface thermal properties using scanning thermal microscopy (SThM), Microsc. Microanal. 22 (6) (2016) 1270–1280.
[53] T. Tanaka, M. Kozako, N. Fuse, Y. Ohki, Proposal of a multi-core model for polymer nanocomposite dielectrics, IEEE Trans. Dielectr. Electr. Insul. 12 (4) (2005) 669–681.
[54] T. Tanaka, G. Montanari, R. Mulhaupt, Polymer nanocomposites as dielectrics and electrical insulation-perspectives for processing technologies, material characterization and future applications, IEEE Trans. Dielectr. Electr. Insul. 11 (5) (2004) 763–784.
[55] A. Arbuzov, V. Muradyan, B. Tarasov, E. Sokolov, Preparation of Amino-Functionalized Graphene Sheets and Their Conductive Properties, Sumy State University, 2013.